Clemson University

TigerPrints

All Theses   Theses

8-2013

Spectroscopic Investigation of Protein Corona

Poonam Choudhary
Clemson University, poonamc@clemson.edu

Follow this and additional works at: https://tigerprints.clemson.edu/all_theses

Part of the Physics Commons

Recommended Citation

SPECTROSCOPIC INVESTIGATION OF PROTEIN CORONA

A Dissertation
Presented to
the Graduate School of
Clemson University

In Partial Fulfillment
of the Requirements for the Degree
Master of Science
Physics

---

by
Poonam Choudhary
August 2103

Accepted by:
Dr.Apparao M Rao, Committee Chair
Dr. Frank Alexis
Dr. RamaKrishna Podila

ABSTRACT

Nanotechnology has revolutionalized the landscape of modern science and technology, including materials, electronics, therapeutics, bioimaging, sensing, and the environment. Research in the past decade has examined the fate of nanomaterials *in vitro* and *in vivo*, as well as the interactions between nanoparticles and biological and ecosystems using primarily toxicological and ecotoxicological approaches. However, due to the versatility in the physical and physicochemical properties of nanoparticles, and due to the vast complexity of their hosting systems, the solubility, transformation, and biocompatibility of nanomaterials are still poorly understood. Nanotechnology has been undergoing tremendous development in recent decades, driven by realized perceived applications of nanomaterials in electronics, therapeutics, imaging, sensing, environmental remediation, and consumer products. Nanoparticles on entering the blood stream undergo an identity change, they become coated with proteins. There are different kind of proteins present in blood. Proteins compete for getting coated over the surface of nanoparticle and this whole entity of proteins coated over nanoparticle surface is called Protein Corona. Proteins tightly bound to the surface of nanoparticle form hard corona and the ones loosely bound on the outer surface form soft corona. This dissertation is aimed at spectroscopic investigation of Protein Corona.

Chapter I of this dissertation offers a comprehensive review of the literature based on nanomaterials with the focus on carbon based nanomaterilas and introduction to Protein Corona. Chapter II is based different methods used for Graphene Synthesis,

different types of defects and doping. In Chapter III influence of defects on Graphene Protein Corona was investigated. Chapter IV is based on the study of Apoptosis induced cell death by Gold and silver nanoparticles. In vitro study of effect of Protein Corona on toxicity of cells was done.

ACKNOWLEDGEMENTS

I would like to thank my advisor, Prof. Apparao M. Rao for his endless support and guidance. His confidence in me helped me complete my research. I have learnt a lot from him and he continues to inspire me to do better in my work. Some of the work done in this thesis would not have been possible without the insights of Dr. Ramakrishna Podila and Dr. Frank Alexis. I am also thankful to Dr. Skove for helping me write my thesis.

I also thank my good friends in Clemson who were always there to support me. And a big thanks to my labmates who helped me in honing my lab skills.

TABLE OF CONTENTS

Page

LIST OF TABLES

LIST OF FIGURES

CHAPTER ONE

LITERATURE REVIEW

1.1 Introduction

The idea of nanotechnology was identified by R.Feynman in his talk "There is plenty of room at the bottom" at the American Physical Society meeting in 1959.Feynman proposed the idea of building machines on the scale of molecules, a few nanometers wide-motors, robot arms, and even whole computers, far smaller than a cell. As nanotechnology became an accepted concept, the meaning of the word shifted to encompass the simpler kinds of nanometer-scale technology. The U.S. National Nanaotechnology Intiative was created to fund research on anything smaller than 100 nanometers with novel properties.

The acceptance of nanotechnology by the public has led to research on the applications and implications of nanomaterials, and the development of nanoscale devices now impacts every aspect of human society [1]. For example, ZnO and Ag nanoparticles (Nps) are beingincorporated into coatings, fibers, polymers, first aid bandages, plastics, soap and textiles to provide anti-microbial, anti-bacterial, antibiotic and anti-fungal activity. Similarly, carbon nanotubes, SiO_2 NPs. CdSe quantum dots have been exploited as superconductors, conductors or semiconductors.[2]

Figure 1-1 The diverse applications of Nanotechnology encompass a wide range of fields including optical devices, energy storage, and nanomedicine [2]

The properties of the materials can change dramatically when their sizes are reduced from the bulk level to the nanoscale. The special properties include: quantum confinement in semiconductor materials, surface plasmon resonance (SPR) in metallic materials, and superparamagnetism in magnetic materials. Reactivity of nanomaterials is usually magnified due to the much-increased surface area to mass ratio, such as that found in super catalytic nano-sized titanium particles. Thus, different approaches and strategies have been adopted to utilize the fascinating properties of nanomaterials for a wide range of applications shown in Figure 1-1.

Due to their unique physical and chemical properties and sizes comparable to biological matter, nanomaterials naturally converge with biology to elicit interesting phenomena. With the growth in the biological applications of nanomaterials, a comprehensive understanding of the interactions between nanomaterials and biological systems has become essential to facilitate the applications and mitigate the adverse effects associated with nanomaterials. Such understanding can be achieve integrating physical and biological sciences and nanotechnologies.

As mentioned previously, nanomaterials are being employed widely for applications in nanomedicine and other biological applications including anti-bacterial and anti-microbial coatings. Additonally, the rapid production and the great economical potential of carbon-based nanomaterials warrant the necessity and importance of examining these nanoparticles with respect to their health, environmental, and biological effects and implications. In this thesis, I investigated the interactions between carbon nanomaterials (mainly graphene), Au NPs and biomolecules (including proteins, lipids, and cell culture media) to understand the influence of protein corona formation on the physiological response to nanomaterials. The thesis is organized into four chapters to facilitate the presentation of my experimental findings. A brief introduction to nanomaterials and their interaction with biological systems is presented in chapter 1. In chapter 2, I describe the traditional synthesis methods, the physics of defects in graphene, and some strategies for doping chemically exfoliated graphene sheets. In chapter 3, the influence of defects in graphene on the formation of protein corona will be discussed. In

the final chapter, the use of Au NPs and protein corona on oxidative therapy for cancer is discussed.

<center>1.2 Carbon-based nanomaterials</center>

The first engineered carbon nanomaterial, fullerene C_{60}, illustrated in Figure 1-3 [4]was discovered by Kroto in 1985. . It is a polygon with 60 carbon atoms which form 12 pentagons (5-member ring) and 20 hexagons (6-member ring). The aromatic properties of the molecule give rise to the π electrons present on both the inner and outer surfaces of the molecule [4].
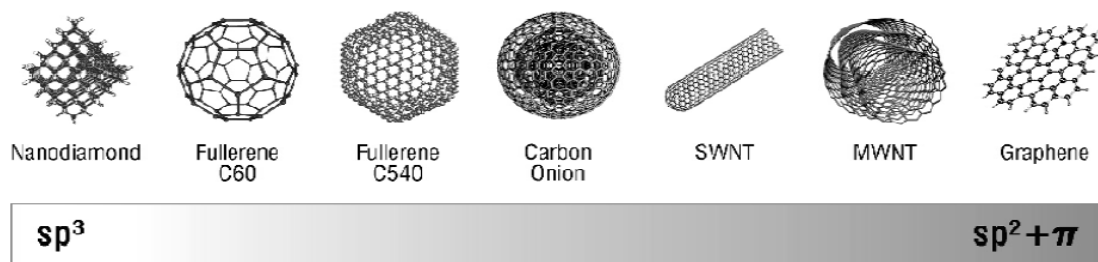
Figure 1-2. Hybridization states of carbon allotropes [5]

The physical, chemical and electronic properties of carbon nanomaterials are directly related to the carbon hybridization state. The orbital configurations of the six carbon electrons assume $1s^2$, $2s^2$, and $2p^2$. Depending upon the neighboring carbon atoms, it can hybridize into sp, sp^2 and sp^3 configurations due to the small energy gap between

the 2s and 2p electron shells. The various hybridizations of carbon lead to the different bulk organizations of each carbon (Figure 1-2). For example, planar graphite carbon atoms assume the form of sp^2 hybridization, with the carbon bonds bent to form a closed sphere or tube. This step is associated with the change of sp^2-hybridized carbon bonds into sp^3-hybridized bonds, resulting in a decrease in the bond angles from 120º to 109.5º. Therefore, the carbon molecule becomes more stable, due to the decrease in bond angle, which bends less when closed into a spherical or tube structure. Structures with a smaller number of hexagons exhibit a greater sp^3 bonding character, higher strain energies, and thus more reactive carbon sites [5]. Therefore, the thermodynamically favorable configuration of carbon is the sp3 diamond configuration. (It is more complicated than that. Graphene is the thermodynamically stable form at room temp. and pressure.) Although C60 is a tiny particle consisting of a cage of 60 carbon atoms with a Vander Waals diameter of 1 nm [4], fullerene molecules in practice crystallize into larger structures. Due to their hydrophobicity, C60 is not soluble in polar solvents, but becomes soluble in selected organic solvents [5]. In order to enhance dispersion, and thus minimize the degree of aggregation, surface modifications are commonly used to enable dispersion of the nanoparticles in aqueous solutions. Water-soluble fullerene derivatives can be obtained by attaching various functional groups (-OH, -COOH, -NH2, etc.), and amphiphilic amoities can be easily adsorbed onto the fullerene cage. Fullerenes can also be solubilized by the adsorption of biomolecules, forming molecular self assembly through non-covalent van der Waals, electrostatic, and hydrophobic interactions [5].

Since the discovery of fullerenes, many more types of carbon nanomaterials have been synthesized for use in commercially available products. These nanoparticles include fullerene [15, 16], carbon nanorods [16], nanofoams [17, carbon dots [16], nanohorns [19], nano-onions [20], and nanodiamonds [22]. Fullerenes - C60, single-walled carbon nanotubes (SWNTs), multi-walled carbon nanotubes (MWNTs) andgraphene are the most widely used types of carbon nanomaterials [23].

1.3 Biological applications of carbon nanomaterials

Considerable efforts have been devoted to the use of nanomaterials in biological applications as well as for improving human health. Examples of such applications include the design of tissue implantable or subcellular sensors [5, 6], drug delivery systems, including gene delivery [7-8], deoxyribonucleic acid (DNA) and ribonucleic acid (RNA), oligopeptides [9, 10], lipids and antibiotics [11], and disease diagnosis and therapy [12-13]. Carbon nanotubes andgraphene can be modified by biomolecules through covalent binding, non-covalent binding, and through a hybrid approach, in which a small molecule 'anchor' is adsorbed on carbon surface, followed by a chemical reaction between the anchor and a biomolecule of interest (Figure 1-3) [14]. Indeed, because carbon nanotubes can be taken up by a variety of mammalian and plant cells, they can be utilized for the delivery of drug and prodrug molecules to living systems.
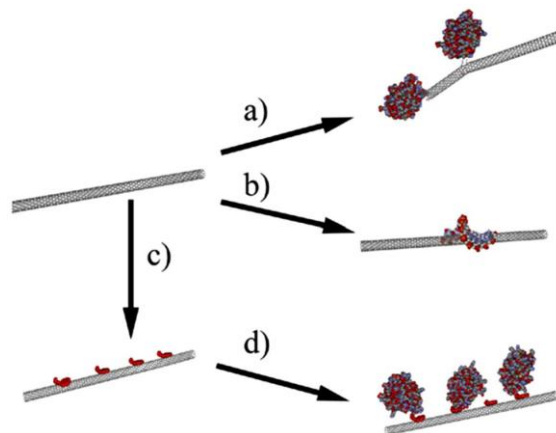
Figure 1-3. Three major approaches to modify carbon nanotubes with biomolecules [15]

Regarding the process of gene delivery, Pantarotto et al. [9] reported the first attempt of utilizing carbon nanotubes for engineering a novel gene delivery system. In their scheme, supramolecular complexes of ammonium-functionalized MWNT and plasmid DNA, formed through electrostatic interaction, were taken by HeLa cells and delivered into cell nuclei with low toxicity. Raman scattering and fluorescence signals of carbon nanotubes and graphene are useful in tracking nanostructures within biological samples, since SWNTs and graphene exhibit distinguished peaks in the Raman and fluorescence spectrum. Thus, near-infrared fluorescence microscopy at wavelengths above 1100 nm provides high contrast images, indicating the locations of SWNTs and graphene within the cell. Based upon these principles described above, Heller et al. [4] proposed the use of SWNT as a long term optical sensor in live cells Figure. (1-4). In this study, DNA-SWNTs exhibited resistance to photobleaching and remained functional in live cells for three months, thus enabling long-term live cell imaging. The Raman scattering and fluorescence spectra of DNA-SWNTs were measured from within live as

well as hematoxylin- and eosin-stained cells; upon uptake no changes occurred to the emission spectra of the nanotubes. The nanotubes, which were observed to remain within cells even after multiple cell divisions, were incorporated into the cytoplasmic vesicles and did not enter the nuclear envelope. Transmission electron microscopy (TEM) images and light-microscopy images confirmed the uptake of these nanotube complexes by endocytosis and their perinuclear endosomal localization within the cells.
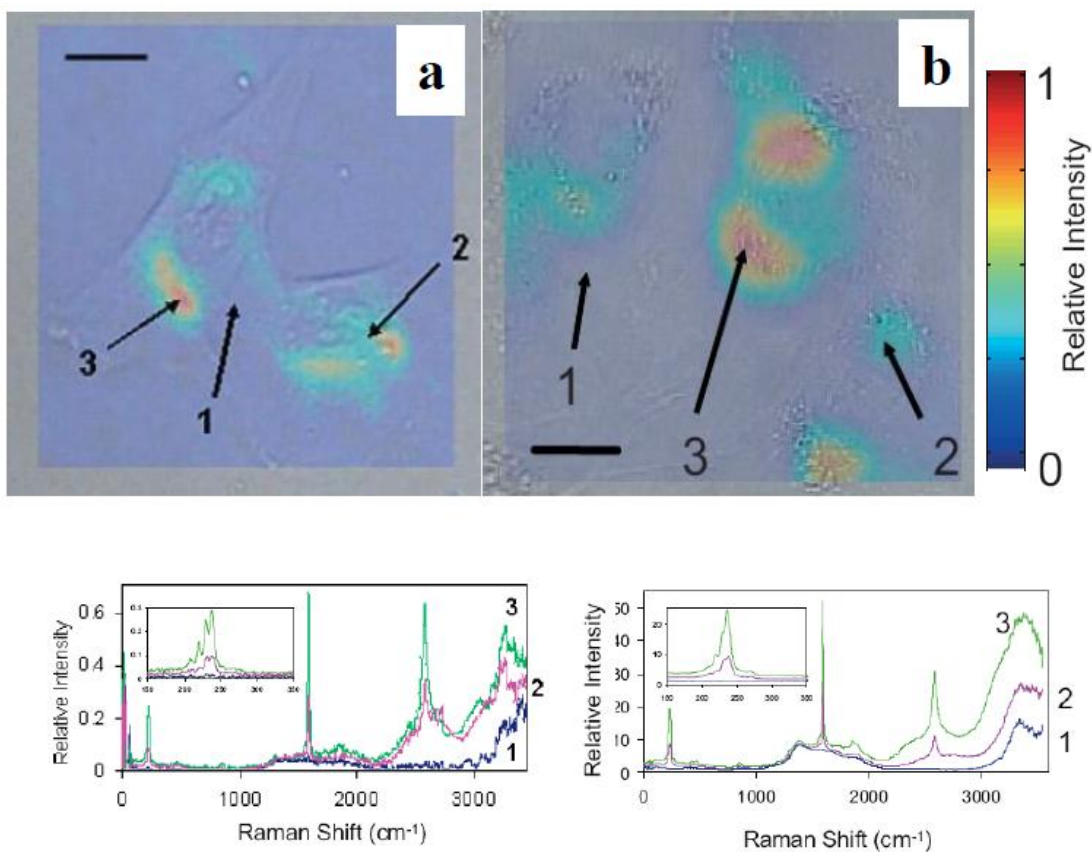
Figure 1-4. Raman intensity area maps of live fibroblast and myoblast stem cells and corresponding spectra [8]: (a) Top: area map of Raman radial breathing modes intensity of SWNTs in live fibroblasts cells after 48 h. in culture overlaid onto an optical micrograph of the same region; Bottom: combined Raman and fluorescence spectra of live murine mouse embryonic fibroblast cells incubated with DNA-suspended SWNTs. The three spectra correspond to locations on the area map: (b) Top: area map of RBM intensity of mouse embryonic fibroblast cells in culture for 8 days; Bottom: Raman and fluorescence spectra of nanotubes in live mouse embryonic fibroblast cells after 8 days.The scale bars represent 20 μm. Color legend is valid for all images.

1.4 Interaction of Nanomaterials with Biological systems

The small size of nanomaterials allows them to enter almost all areas of the body (including cells and organelles) and to cross the blood-brain barrier, thus they are of great use in developing novel drug and gene delivery approaches, and equally hazardous to human health. Human exposure to environmental nanomaterials (ENMs) may occur unintentionally *via* inhalation of airborne ENMs or through the use of nanotechnology enabled products such as nanomaterial-based drug delivery agents. In any case, extensive manufacturing and the use of nanomaterialss have raised concerns regarding their impact on biological response in living organisms, and the environment at large. As the fundamental properties of ENMs are dependent upon a complexity of factors (*e.g.* morphology, size, defects, and chemical stability) elucidating their biological responses with their intricate physicochemical properties is a challenging process. For example, a varying toxic response may manifest in nanomaterials either due to different synthesis routes used in their preparation, dissimilar impurities or the nature of defects. Consequently, these varying responses makes it a monumental challenge to evaluate the health hazards of all ENMs presently used in the global market. Methods for evaluating the health hazards of ENMs currently in use are both expensive and time consuming. Indeed, the individual *in vivo/in vitro* toxicity evaluation for each ENM can cost upwards of one million dollars. Therefore, developing methodologies to predict the physiological response of ENMs based on their physicochemical properties is of great importance.

Recent nanomedical research has been undertaken to elucidate the fundamental problems of nanostructure surface 'fouling' or opsonization that occurs with the formation of protein coating or 'corona' Figure 1-5 [19]. The nanoparticle-protein corona (NP-PC) is known to trigger physiological and pathological changes including protein aggregation, blood coagulation and complement activation. In addition, the NP-PC can compromise the targeting capacity of functionalized nanoparticles and subsequently negate any therapeutic potential. There is also compelling evidence that the physiological responses to nanomaterials in a biological medium reflect the adsorbed biomolecule layer, rather than the ENMs itself. Therefore, the biomolecular layer can either promote or mitigate toxicity, via direct biodistribution of nanomaterials within a biological system to either improve or impair delivery of nanomedicines. A detailed understanding of the NP-protein interactions, which are described in my thesis, will support ongoing research into the biosafety of nanomaterials.
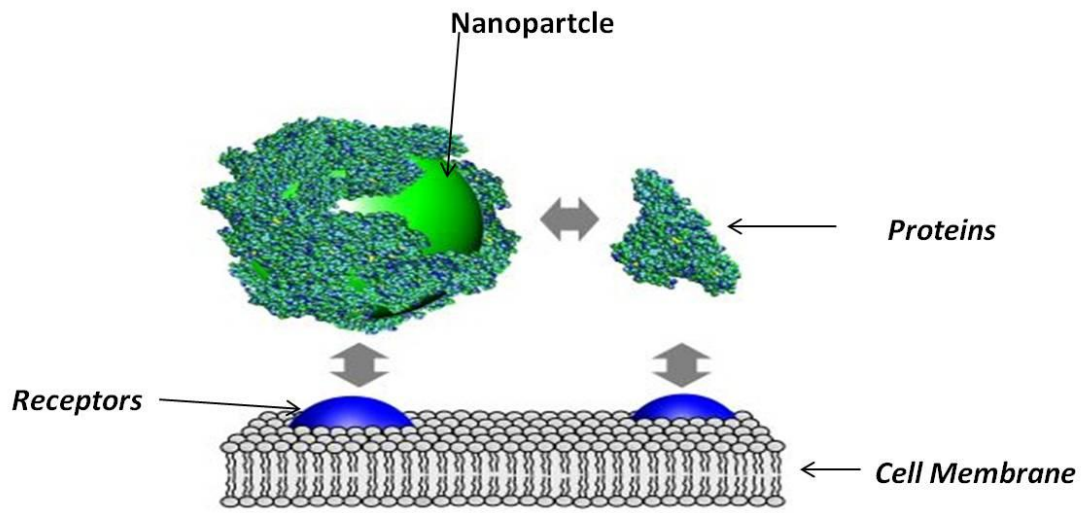
Figure 1-5 Proteins (blue-green) enclose a nanoparticle (green) that can bind to the cell membrane, *e.g.*, to receptor proteins (blue) [19]

CHAPTER-TWO

GRAPHENE SYNTHESIS AND DOPING

2.1Graphene

Graphene is a two-dimensional sheet of sp^2 bonded carbon atoms arranged in a hexagonal lattice. Figure.2-1 shows two different triangular sub-lattice structures A and B that combine to form a honeycomb lattice. The distance between nearest neighbor carbon atoms is about a = 1.42 Å, which is the average of the single (C-C) and double (C=C) bond and strongly bonded by σ bonds. The other bond which is oriented in the direction out of the plane is the π bond. These π orbitals can be visualized as a pair of symmetric lobes oriented along the z-axis and centered on the nucleus. Each atom has one of these π-bonds, which are then hybridized together to form what are referred to as the π-band and π∗-bands.
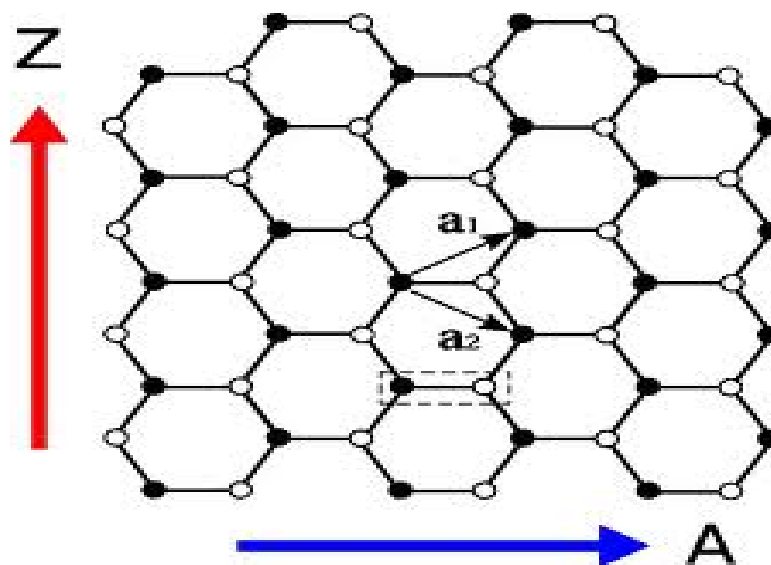
Figure 2-1 The graphene honey-comb lattice showing A and B sub-lattices and the graphene lattice vectors.

2.2 Graphene Synthesis Methods

2.2.1 Mechanical exfoliation

Graphene was first obtained from bulk highly ordered pyrolytic graphite (HOPG) by mechanical exfoliation (repeated peeling) using scotch tape [24-26]. Layers in bulk graphite are held together by a force of about *300 nN/μm²* [27] Such a small force can easily be managed by adhesive tape. After repeated peeling, the graphene from the adhesive tape can be transferred to a SiO_2/Si substrate by gentle pressing[25,26]. To distinguish between layers of graphene, the thickness of the SiO_2 is important because at the thickness of *90 nm* or *280 nm*, the opticalcontrast of graphene on SiO2 is maximized by about *12%* at *550 nm* where the sensitivity of human eye is optimal [27]. Fig. 2-2.

shows optical image of graphene transferred by mechanical exfoliation onto ~ *300 nm*

SiO_2. Yellow regions in Fig. 2-2 (a) represent thin graphite layers of the order of *100 nm*

and the light purple regions in Fig.2-2 (a) and Fig.2-2 (b) shows monolayer graphene [28]
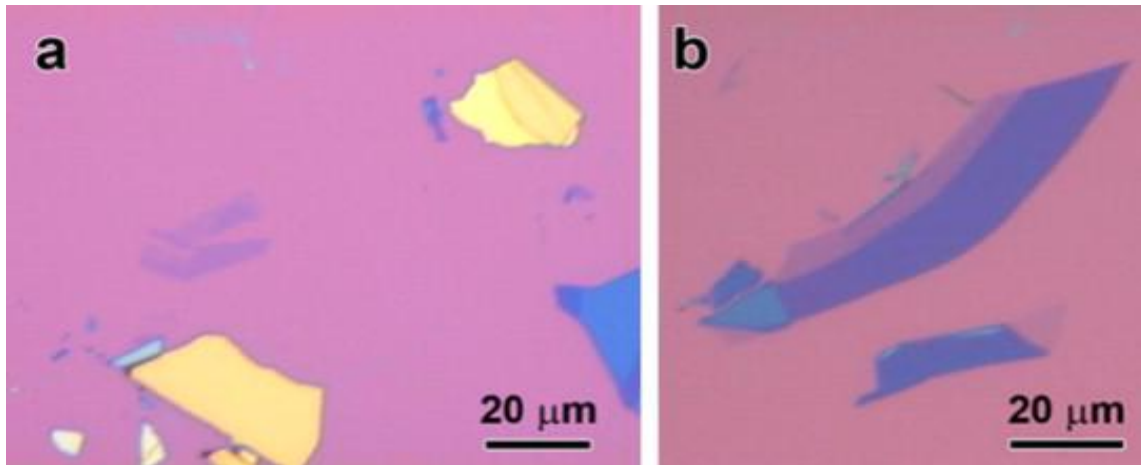
Figure 2-2. Micromechanically exfoliated graphene. Optical images of (a) thin layer graphite and(b) Few layer graphene (FLG) and single layer graphene (light purple contrast) on ~ *300 nm* SiO2

2.2.2 Graphitization of silicon carbide

Silicon Carbide (SiC) is a highly resistive material. When heated around 1400°C under

vacuum, the silicon sublimes resulting in a layer of graphite [31]. The problem with high

temperature vacuum annealing of SiC is that it results in highly corrugated surface

covered by small graphene regions with varying thickness [32]. One solution to this

problem was to use C terminated SiC instead of the previously used Si terminated SiC.

This resulted in improved graphene coverage of the order of 1 μm [33]. However much

higher graphene coverage with this method was achieved by graphitization near

atmospheric pressure under Ar ambient that resulted in smooth surface with graphene coverage as large as 50 μm [34]. The reason for this improved coverage was the more sublimation of silicon atoms due to higher temperature around 1650°C under Ar ambient at near atmospheric pressure [32,34]. The graphene obtained by this method showed field effect mobility only five times smaller than exfoliated graphene [34].

2.2.3 Wet chemical route

The basic idea behind this technique is to intercalate layers of graphite derivates with different reactants that results in the separation of these layers from the bulk. The precursor is usually graphite which is first reacted with strong acids and oxidants to produce graphite oxide [33]. As a result of this reaction, various hydroxyl and epoxide groups attach to the carbon atoms in graphite oxide through covalent bonds [36,37] with the result that though original layered structure of graphite is retained, but the conjugated structure of carbon atoms is severely distorted [35]. Graphite oxide is thus a layered structure of graphene oxide sheets that do not preserve the original conjugated bond structure of graphite [37]. An attempt to reduce graphene oxide with various reducing agents e.g. hydrazine, dimethylhydrazine and hydroquinone result in colloidal suspension of varying conductivity and graphene flakes of different lateral sizes and thickness [35]. The challenge in this approach is that the original structure of graphite is modified and even after treatment with reducing agents, the original sp^2 network of carbon atoms in not restored. To overcome this problem, non covalent functionalization of the conjugated carbon network in graphite is achieved through 1-pyrene carboxylic acid [39] and 9-

16

anthracene carboxylic acid [40The advantage of this scheme is that external functional groups attach to the carbon network through π-π stacking rather covalent bond formation. As a result of π-π stacking, the conjugated network of sp2 bonded carbon atoms in graphite is retained and the obtained graphene flakes shows improved electrical properties [40]. Though non covalent functionalization improves the electrical properties of the resulting graphene flakes, the scalability of this method to wafer scale is still challenging.

2.2.4 Chemical vapor deposition

The essence of this technique is that precursors in the vapor phase adsorb and react at the substrate surface at elevated temperatures under low pressure (of the order of milli torr) or atmospheric pressure that results in the deposition of thin film as a result of chemical reaction. In the case of graphene synthesis, precursors are usually carbon containing gas e.g. methane or vapors of any liquid carbon source e.g. alcohols that react on the transition metal surface under the ambient environment (e.g. Ar to avoid deposition of amorphous carbon). Commercial copper foils have been used forgraphene synthesis to reduce the overall cost of fabrication process but these foils have a strongly corrugated surface due to a cold rolling process during manufacture and this surface roughness is known to produce graphene thickness variations on copper [42,41]. Since graphene growth on copper is surface limited, the smoothness of the copper surface plays a very important role in getting monolayer coverage across the entire surface of the substrate [44,42].
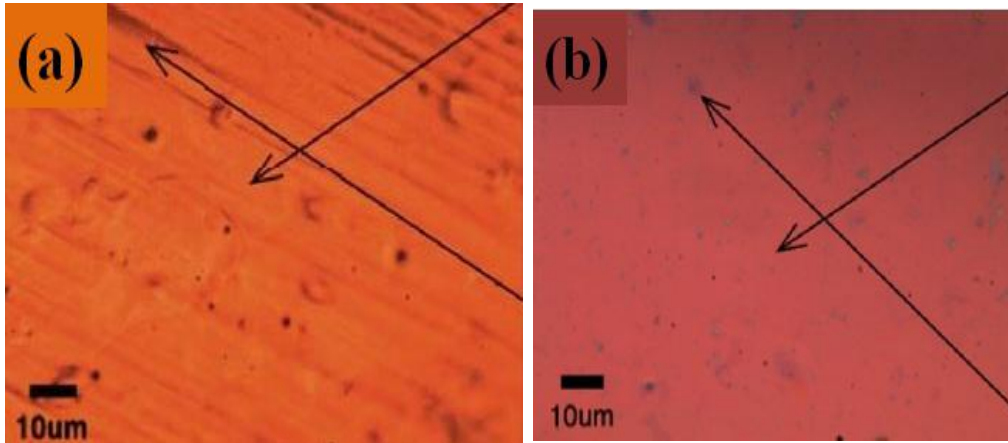
Figure.2-3. CVD grown graphene on copper. Optical images of (a) as-grown graphene and (b)transferred to *300 nm* SiO$_2$. Black arrows in (a) show corrugations on copper surface that results in multilayer graphene highlighted by black arrows close to purple regions in (b) [43].

2.3 Defects in Graphene

Defects in three-dimensional crystals are referred to as *intrinsic* when the crystalline order is perturbed without the presence of foreign atoms. The latter are denoted as impurities and constitute *extrinsic* defects. In macroscopic crystalline materials, intrinsic defects have different dimensionalities. Point defects, typically vacancies or interstitial atoms, are zero dimensional,whereas the concept of dislocations is based on one dimensional lines of defects. Grain boundaries or stacking faults extend in two dimensions, while inclusions and voids have a finite size in all three dimensions. Foreign atoms may exist as zero-dimensional defects when they substitute for individual

atoms of the crystal or are located on interstitial sites. On the other hand, agglomerations of foreign atoms can extend to more dimensions.

2.3.1 Point Defects

StoneWales defect - As mentioned above, one of the unique properties of the graphene lattice is its ability to reconstruct by forming nonhexagonal rings. The simplest example is the Stone-Wales (SW) defect [38] which does not involve any removed or added atoms. Four hexagons are transformed into two pentagons and two heptagons[37-40]defect by rotating one of the C_C bonds by 90°, as shown Figure 2-4
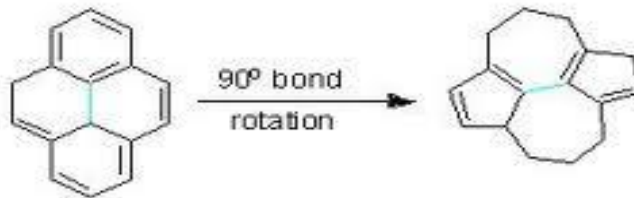
Figure. 2-4 Shows 90°rotation in C-C bond

2.3.2 Single and Multiple Vacancies

The simplest defect in any material is a missing lattice atom which forms a Single Vacancy Figure 2-5 (a). Double vacancies (DV) can be created either by the coalescence of two SVs or by removing two neighboring atoms as shown in Figure 2-5 (b).The atomic network remains coherent with minor perturbations in the bond lengths around the defect.

(a)   (b)
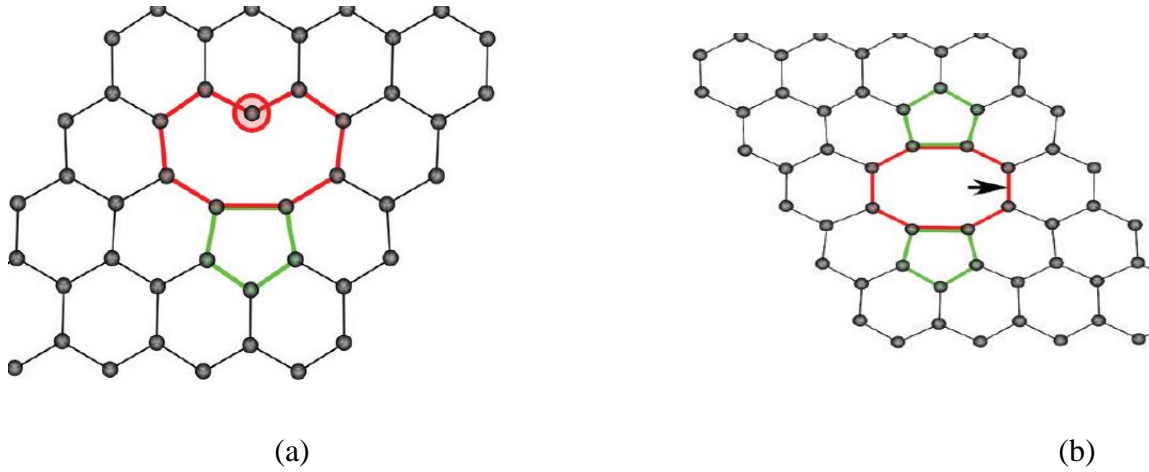
Figure 2-5 (a) Single vacancy (b) Multiple vacancy

2.3.4 Foreign Adatoms

The effect of a foreign (noncarbon) atom on the properties of graphene depends on the bonding between the atom and graphene [34] If the bond is weak, only physisorption due to van der Waals interaction occurs. If the interaction is stronger, covalent bonding between the foreign atom and the nearest carbon atoms leads to chemisorption. Various bonding configurations exist, normally corresponding to high symmetry positions, such as on top of a carbon atom, or on top of the center of a hexagon, or the bridge position.
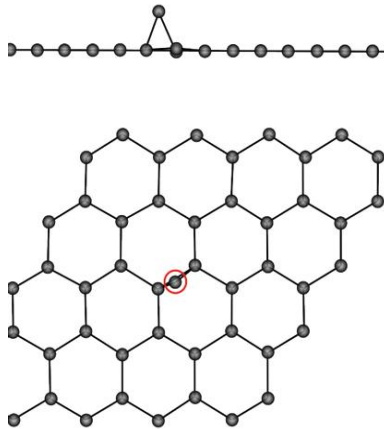
Figure 2-6 Shows foreign single adatom on the bridge

2.3.5. Substitutional Impurities

Foreign atoms can also be incorporated into graphene as substitutional impurities. In this case, the impurity atom replaces one or two carbon atoms. Boron, sulphur and nitrogen serve as the natural dopants in carbon structures since they have one electron less or more, respectively, but roughly the same atomic radius. Sulphur doping that was done in the lab as a part of my side project is described in next section.

2.4 Sulphur Doping

Graphene nanopellets of 1 gm mass were purified in HCL for 48 hours under water bath and then H_2O_2 was added slowly on the third day for another 24 hours. This procedure was done to introduce defects in graphene nanopellets so that the sulphur could take the place of the spots where defects were introduced. After 36 hours of purification graphene nanopellets were filtered using a vaccum pump and filter paper. Graphene nanopellets were then dried in the oven at 60°C for about two hours. The next step was to add sulphur to the graphene nanopellets. Three sets of of sulphur and graphene nanopellets were weighed by molecular mass ratio and were mixed together. After thorough mixing , the mixture was put in a sealed vacuum tube and kept in the oven for 24 hours at 1000°C. Then tube was half inside and the other part was kept outside for another 24 hours so that extra sulphur can sublime to the other end. After 24 hours of thisprocedure the tube was broken and the sample collected and sent for XPS studies.

CHAPTER-THREE

INFLUENCE OF DEFECTS ON GRAPHENE PROTEIN CORONA

FORMATION

3.1 Introduction

The field of nanotechnology is progressing at a rapid rate due to the remarkable potential of nanomaterials for numerous applications in electronics, chemical, biological, and medical fields. As such the global market for nanotechnology-enabled products is now predicted to top 100 billion dollars per annum for 2011–2015 [2]. Further, because the small size of nanomaterials (NM) allows them to enter almost all areas of the body (including cells and organelles) and to cross blood-brain barrier, they are of great use in developing novel drug and gene delivery approaches, and equally hazardous to human health. Human exposure to NM may occur unintentionally in the environment via inhalation of airborne NMs or through the use of nanotechnology-enabled products such as NM-based drug delivery agents. In any case, extensive manufacturing and the use of NMs have raised concerns regarding their impact on biological response in living organisms, and the environment at large.[3].As the fundamental properties of NMs are dependent upon a complexity of factors (e.g. morphology, size, defects, and chemical stability) elucidating their biological responses with their intricate physicochemical properties is a challenging process. It has been previously established that the reticuloendothelial system integrates NMs due to the adsorption of certain serum/complement proteins called 'opsonins'.[45] Upon exposure to serum or plasma,

NMs rapidly adsorb protein molecules leading to the formation of a protein "corona".[10]The adsorption of proteins on NPs occurs mainly due to: i) an increase in the collective entropy of the proteins on an NM surface and ii) nonspecific interactions between the NM surface and the proteins (for example, pi-pi stacking). In other words, the formation of protein corona has been found to depend largely on the physicochemical characteristics of the NMs, in addition to that of the proteins themselves. [11-13] Therefore, it is pertinent to understand the role of NM physicochemical properties in the formation of protein corona. Most importantly, it is well known that the structural defects in NM interact strongly with biological entities due to the presence of localized charged centers. Indeed, charged defects have been proposed to be the common denominator in the physiological response of completely unrelated chemicals. Herein, we have investigated the influence of structural defects on the formation of protein corona by studying the interactions between serum albumin and few-layer graphene (FLG). We have chosen graphene primarily due to its increasing production and high potential for applications in nanomedicine and serum albumin since it is one of the dominant proteins in blood. We synthesized FLG via chemical exfoliation technique and induced different amounts of defects using continuous ball-milling/tip sonication and acid treatment. We quantified the defects in FLG using Raman spectroscopy. Interestingly, we observed that the amount of protein coating increases concomitantly with increasing defects in graphene suggesting that defects can play a crucial role in designing non-sticky nanomaterials resistant to protein coating. We explain our results in terms of defect-induced variations in the hydrophilicity of graphene.

3.2 Materials and Methods

Pristine graphene was synthesized using chemical vapor deposition (CVD). and exfoliated graphene was prepared by chemical exfoliation. [25-27]. For CVD, 25 μm Ni foils were placed away from the center of the tube furnace (diameter: 24 mm), which was maintained at 900 °C under a flow of Ar (230 sccm) and H2 (120 sccm) [73]. After 60 min, Ni foils were moved to the center, and graphene was synthesized by decomposing methane (10 sccm) for 10 min at a reduced temperature (850°C). Subsequently, methane flow was shut off and the samples were moved away from the center. The furnace temperature was ramped down to 400°C at 5°C/min and was maintained at 400°C for 90 min. The H2 flow was shut off immediately upon reaching 400°C, and the samples were cooled down to room temperature under Ar flow. For solvent exfoliation of graphene, bulk graphite (~1 g) was dispersed in 100 mL of N-methyl-2-pyrrolidone (NMP) and sonicated using 1/8 in tip sonicator (Branson 250) at 100 W for 2 h. The resulting dispersion was filtered through 0.45 μm nylon filter and resuspended in 100 mL of fresh NMP. Subsequently, the solution was bath sonicated for 6 h and centrifuged at 500 rpm for 45 min. The supernatant was vacuum filtered using a 0.45 μm nylon filter. Finally, the filtered powder was washed several times using deionized water to remove residual NMP. Graphene treated with acid was prepared by treating Graphene pellets with H2SO4 for 24 h. For protein binding, three samples of 5 ml graphene (1 mg/ml) were added to 5 ml of BSA solution and bath sonicated for 5 min to achieve dispersion. These dispersions were incubated at 37°C. After 1 h of incubation, the samples were centrifuged (at 1500

rpm for 15 min), and the obtained pellets were washed in deionized water and then resuspended .Three such wash steps were employed in order to remove any soft corona and unadsorbed BSA. Finally, the pellets were washed and resuspended in water for UV−vis absorption studies. The aforementioned rigorous wash steps were necessary to remove any unbound albumin and confirm the hard corona of the protein. For Raman, the graphene pellets were vaccum filtered and dried. UV−vis absorption measurements were performed using a PerkinElmer Lambda 950 spectrometer. Raman spectra were collected using a 364 Dilor XY triple grating spectrometer equipped with TE cooled CCD coupled to an Ar+ laser excitation at 514.5 nm. Zeta potential measurements were done by using a Malvern Zetasizer.

3.3 Results and Discussion

3.3.1 Scanning Electron Microscopy

The Chemical Vapor Deposition (CVD) method yielded polycrystalline graphene that mimicked Ni crystal grains, as shown in the Figure 3-1 (a) image. After incubating in BSA solution for an hour, graphene grains were not as clearly visible as in the pristine sample due to significant coverage of the proteins on the substrate Figure.3-1 (a). As seen in Figure3-1 (b) the adsorbed protein form islands on the flat surface graphene. The significant white spots visible in the image are evidence of coverage of BSA on graphene. This coverage of BSA over the surface of graphene could be due to strong covalent, hydrophobic interactions between graphene and BSA.
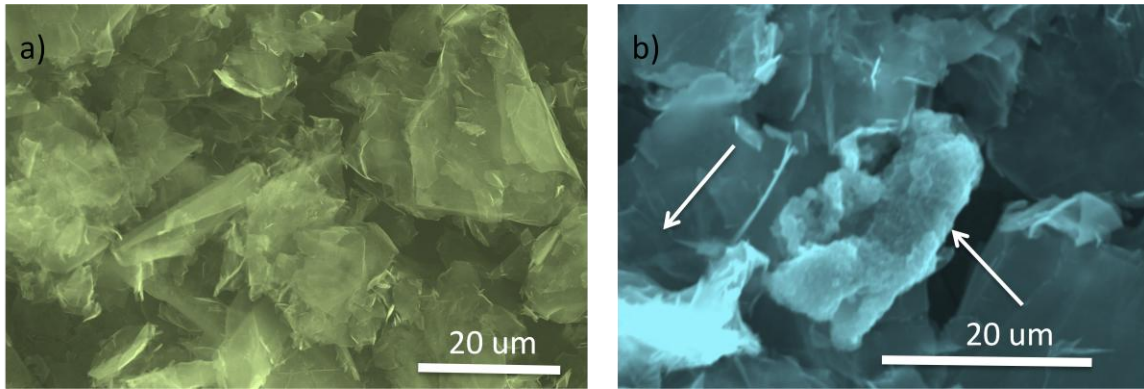
Figure 3-1.(a) SEM images of Pristine Graphene (scale bar: 20 µm) (b) SEM image of Pristine Graphene after incubation with BSA for 1 hour. The arrows on white spots clearly indicates the BSA coated Graphene (scale bar: 20µm)

3.3.2 Raman Spectroscopy

Graphene's electronic structure is captured in its Raman spectrum. Raman fingerprints for single layers, bilayers, and few layers reflect changes in the electron bands and allow unambiguous, high-throughput, nondestructive identification of graphene layers and defects. As shown in Figure 3-2 (a), the main features in the Raman spectra of carbons are the so called G and D (defect) peaks, which lie at around 1560 and 1360 cm^{-1} respectively for visible excitation. The G peak is due to the bond stretching of all pairs of sp^2 atoms in both rings and chains. The D peak is due to the breathing modes of sp^2 atoms in rings [4]. The D peak increases in amplitude from Graphene I to Graphene III implying that garphene treated with acid had the highest number of defects as compared to exfoliated and pristine graphene. Figure 3-2 (b) shows higher value Id / Ig ratio for the graphene treated with acid. Here Id represents the amplitude of the intensity of D peak and Ig represents the amplitude of intensity of G peak.

27
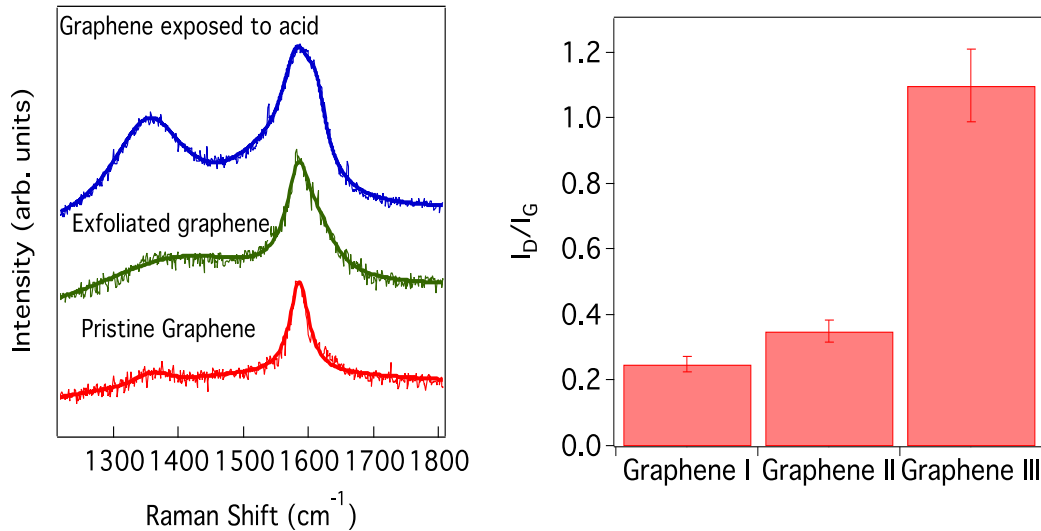
Figure 3-2 (a) Raman Spectra of Pristine, Exfoliated and Graphene exposed to acid before being incubated with BSA. They clearly exhibit a Lorentzian line shape. (b) shows Id/Ig ratio indicating that Graphene exposed to acid has the highest number of defects followed by Exfoliated Graphene and Pristine Graphene. Graphene I – Pristine Graphene, Graphene II – Exfoliated Graphene, Graphene III – Graphene treated with Acid

3.3.3 UV-Vis Spectroscopy

BSA (Bovine Serum Albumin) shows its characteristic absorbance peak at 280 nm as shown in Figure 3-3 (a). The amplitude of the absorbance peak increases with the increase in concentration as expected. The standard curve in Figure 3-3 (b) shows a linear trend, clearly showing that the amplitude of the signal increases with increase in concentration. Figure 3-3 (a) shows the UV-Vis absorption spectrum of the three samples of Graphene incubated with BSA for 1 hour. After centrifugation and washing three times it is evident from Figure 3-3 (c) that BSA manages to from strong bonds with graphene. These bonds can be hydrophobic or electrostatic in nature. The hydrophobic moieties in the structure of BSA interact with graphene as it is also hydrophobic in

28

nature. However, it is worthy to note that the amplitude of UV-Vis signal increases from

Graphene I (Pristine Graphene) to Graphene III (Graphene treated with Acid) clearly

pointing towards the fact that BSA was retained more on Graphene treated with acid. In

other words, the more the number of defects, the more is the interaction with BSA.

During the process of manufacturing exfoliated graphene and also when graphene is

treated with acid, the pristine structure of sp2 hybridisation is disturbed and different

types of defects are introduced in two or three layered graphene [15]. These defects affect

electronic, mechanical and optical properties of graphene considerably [16]. Due to the

introduction of these defects, stronger interaction with BSA is possible, which leads to

more BSA retained on them. It is evident in Figure 3-3 (d) that graphene treated with acid

has more BSA retained on it resulting from strong electrostatic interactions between

defects and aromatic tryptophan present in BSA. Hydrophobic interactions might be due

to interactions between hydrophobic moieties of BSA and hydrophobic edges of

graphene [58-60]
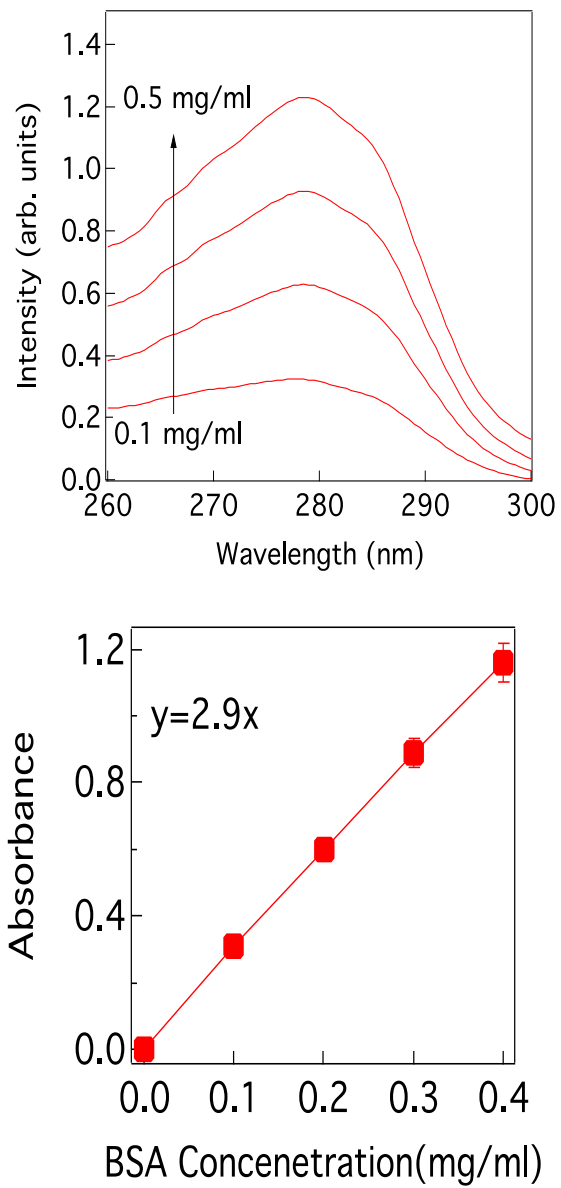
Figure 3.3(a) Shows UV-Vis absorption spectra of BSA concentrations ranging from 0.1 mg/ml 0.5mg/ml. (b) Standard absorption curve shows a linear trend increasing with the increase in concentration.
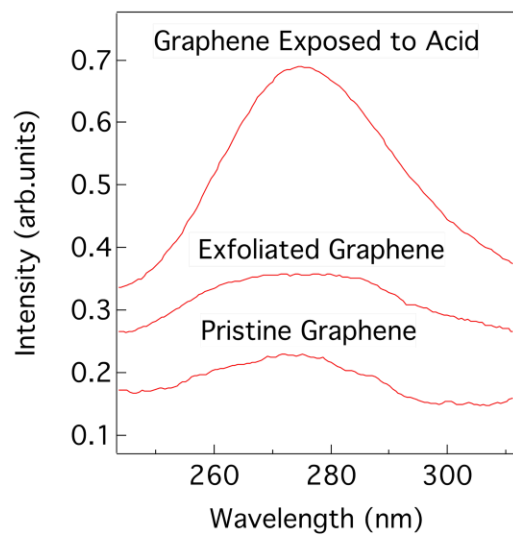
(c)
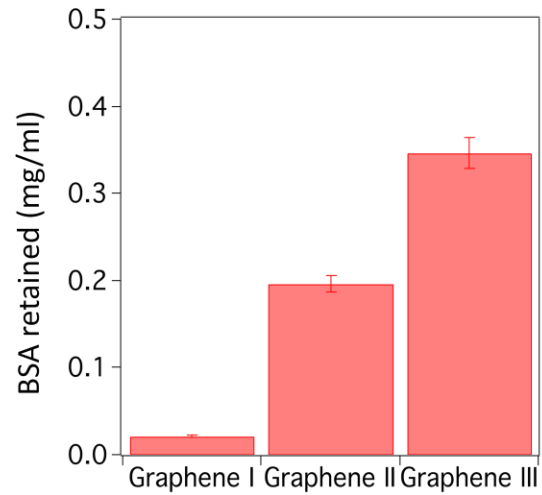
(d)

Figure 3-3 (c) Shows the UV-Vis absorption spectra of the samples after incubation with BSA for 1 hour and centrifugation and washing three times. (d) The amount of BSA retained on graphene after three times of centrifugation and washing clearly showed that Graphene with more defects had more BSA retained on it

3.3.4 Zeta Potential

Zeta potential is a physical property exhibited by any particle that is in a suspension. The zeta potential value gives a measure of the stability of the solution. A layer of ions that are surrounding any charged particle in a suspension is called the Stern layer. The layer outside the Stern layer is called the diffuse layer, in which the ions are not as strongly bonded to the core. Within this diffuse layer, an imaginary boundary called the slipping plane exists, in which ions move with the particle when a voltage is

applied but the ions outside this remain inert as shown in Figure 3-4. The potential at

such a boundary is called the Zeta potential.

.
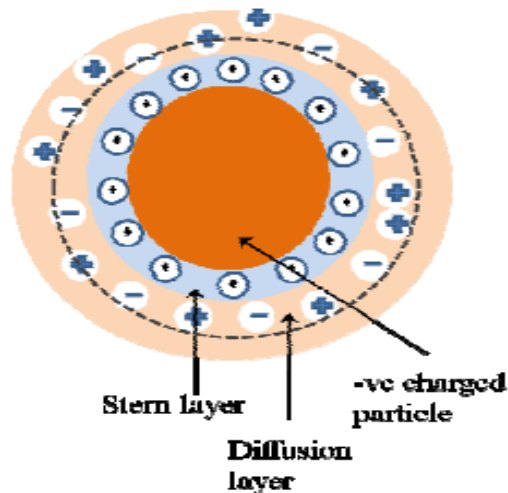
Figure 3-4 Schematic representation charge distribution around a negatively charged
particle

Table 3-4 Shows the zeta potential values of the three graphene samples. Pristine

graphene has the lowest negative potential of 23.1 mV, implying that it forms the most

unstable dispersion in water. These values of the Zeta potential clearly shows that

defective graphene samples form stable dispersions. This again could be attributed to the

fact that the defects paves the way for more electrostatic interactions between water and

graphene as more sites are avialable on the surface of graphene [58]. Pristine graphene

when mixed with SDS (sodium dodecyl sulfate) which is a well known solvent medium

of CNT's and graphene showed the value of - 43.21 mV which is much closer to the

values of zeta potential of the defective graphene in water clearly showing that graphene

with defects forms more stable solution as compared to the graphene with lesser defects

[59].

Sample	Zeta Potential(mV)
Pristine Graphene	-23.1
Exfoliated Graphene	-40
Graphene treated with Acid	-42
Pristine graphene + SDS	-43.29

Table 3-4 Zeta Potential of different samples of Graphene

3.4 Conclusions

In summary, we found that the defects in graphene structures, regardless of the source and type, influence their dispersion ability and hence, affect their tendency to interact with proteins. More BSA was retained on graphene with more defects. The I_d / I_g ratio of graphene treated with acid was highest which could be due to hydrogen bonds formed as a result of bond cleavage in the C-C network. Therefore, pristine graphene is probably a more useful candidate for biomedical applications depending on the needs.

CHAPTER-4

APOPTOTIC CELL DEATH BY GOLD AND SILVER NANOPARTICLES

4.1 Introduction

The ability to tailor and engineer nanomaterials with desired physicochemical properties has resulted in numerous applications in chemical, biological, and medical fields. Particularly, nanomaterials have shown promising solutions for cancer diagnosis, therapy, molecular targeting, drug delivery and many other biomedical applications[67]. In view of this, the United States National Cancer Institute (NCI) launched the 'Alliance for Nanotechnology in Cancer' in 2004 to accelerate research in cancer nanotechnology and promptly achieve clinical applications. Nanoparticles (NPs) are being widely used for oxidative therapy against cancer [67] . NP-based oxidative cancer therapy involves the elimination of free oxygen radicals that are involved in multistage carcinogenic process. Any oxidative DNA damage by free oxygen radicals and suppressive effects on DNA repair can propel carcinogen activation ensuing in tumor promotion [51]. Furthermore, oxidative damage can initiate programmed cell death or apoptosis. As a result of apoptosis, the DNA machinery is halted due to modifications produced in cellular chromatin.

Reactive Oxygen Species (ROS) can cause DNA modifications in the histones and thereby change the conformation of the DNA-binding sites. As a result, the DNA molecule is further exposed to oxygen radicals that destabilize the helix leading to cell death [49]. It is clear that there exist a plethora of interrelated mechanisms in cancer cells,

which can be exploited for employing different treatment strategies. Accordingly, various strategies such as chemotherapy, hyperthermia, and radiation therapy have been developed [66]. Many in vitro studies have studied the effects of noble metal nanoparticles on apoptosis in order to develop novel NP based oxidative therapeutic strategies against cancer. However, the effects of non-specific binding of proteins to NPs or NP-surface fouling on apoptosis have not yet been well investigated.

Surface fouling and subsequent formation of a so-called 'protein corona' can mediate the uptake of the NPs via receptor-mediated endocytosis. The main blood plasma proteins involved (both directly and indirectly) in surface fouling are albumins, fibronectins, complement proteins, fibrinogen, immunoglobulins and apolipoproteins. Surface fouling has been found to result in phagocytosis of the nanostructure by monocytes/macrophages ultimately promoting an immune response and inflammation. In the presence of protein corona, particle-cell interaction depends on the type of coated protein(s), electronic charge, and protein-lipid interactions [53-55]. It is well known that the adsorption of proteins onto the NP surface occurs mainly due to a gain in conformational entropy (DS) due to protein unfolding. Therefore, any conformational changes that occur in the protein upon binding NPs can also cause adverse physiological response. In light of this, it is pertinent to study the effects of protein corona formation on the physiological response of NPs.

Here, we studied the effects of protein corona formation on the physiological response of gold and silver NPs (GNPs and AgNPs) in three different cells lines breast (MCF-7), colorectal (HT-29), and prostate cancer cells (DU-145). We investigated the

dependence of physicochemical properties on the formation of albumin and fetal bovine serum protein corona using UV-Visible spectrophotometry, dynamic light scattering, and gel electrophoresis. Our results indicated that apoptosis is dependent on the size of the NPs. More importantly, our studies showed that protein corona causes significant changes in the induction of apoptosis due to several factors such as reduced surface charge, change in protein conformation, and increased agglomeration.

<div align="center">4.2 Materials and Methods</div>

DU-145 cells were grown in Dulbecco's modified Eagle's 100 medium (DMEM) modified to contain Earles Balanced Salt Solution, non-essential amino acids, 2 mM L-glutamine, 1 mM sodium pyruvate, and 1,500 mg/L sodium bicarbonate. It was supplemented with fetal bovine serum to a final concentration of 10 %, 100 UI/ml penicillin G, and 100 μg/ml streptomycin. The cells were grown in a humidified incubator with 5 % of CO_2 at 37 °C. All the media components were purchased from Promega, USA. The HT-29 cells were grown in McCoy's medium (ATCC, USA). The MCF-7 cells were cultured in Eagle's Minimum Essential Medium (ATCC, USA).

The commercial gold and silver nanoparticles (GNPs): 20 and 80 nm AgNPs and 20 nm GNPs were purchased from Ted Pella Inc., USA while 80 nm GNPs were prepared using a laser ablation technique. The basic set up of Laser Ablation is shown in Figure 4-1.

Gold Pellet   Lens   Laser
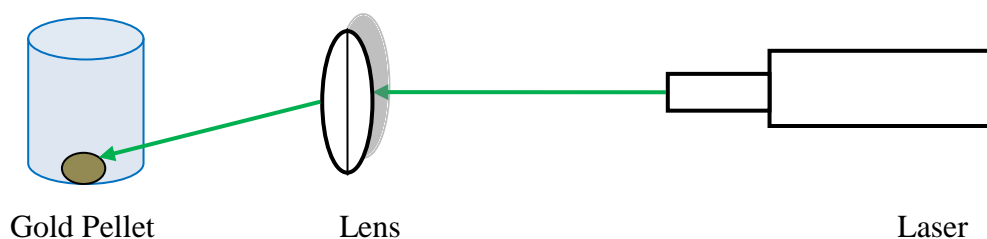
Figure 4-1 Experimental Set up for Laser ablation

For ease of discussion, we labeled NPs as X-GNP/X-AgNP where X indicates the NP size. All NPs were characterized using a Hitachi H-7600 transmission electron microscope. For studying the effects of protein coated NPs on apoptosis, all NPs were coated with Fetal Bovine Serum (FBS) and bovine serum albumin (ALB) using the following procedure. All the samples were incubated in Alb or FBS for 1 h at 37°C. Subsequently, the samples were washed by centrifuging at 10000 g for 10 min. The pellets containing protein coated NPs were washed thrice with nanopure water in order to remove any loosely bound proteins. Finally, all NPs were re-suspended in nanopure water. SDS-PAGE was performed for all the samples using a 4-20% gel (Biorad, USA). The gel was stained by Coomassie blue stain. A Smart Protein standard (Genscript, USA) was used to identify and analyze the presence of BSA and FBS bound to the samples. The hydrodynamic sizes of the plain NPs and protein-bound NP samples were measured using dynamic light scattering (DLS) using Malvern Zetasizer and UV-Vis spectroscopy (Biotek Synergy H2, USA).

Cell death detection ELISA assay: We measured apoptosis using a photometric enzyme immunoassay available in the Cell Death Detection ELISA kit (Roche chemicals, USA). Briefly, the kit is an in vitro technique that measures the cytoplasmic histone-associated DNA fragments (mono- and oligonucleosomes) after induced cell death. The anti-histone antibody reacts with the histones H1, H2A, H2B, H3 and H4. Addition of anti-DNA peroxidase binds to single and double-stranded DNA. Hence, the ELISA allows the detection of mono and oligonucleosomes by measuring the optical absorbance at 405 nm. For all the studies, cells were diluted with culture medium to obtain a 1×10^5 cells/ml concentration in a 96-well plate. Samples containing the commercial plain 20 nm GNPs, 20 nm AgNPs, 80 nm GNPs and 80 AgNPs and the corresponding protein coated (FBS & ALB) NPs were added to the cells. The 96- well plates were incubated for 24 h. The cells were then centrifuged at 200 x g for 5 min. After discarding the supernatant the cell pellet was resuspended in cell culture medium.

Statistical analysis: All experiments were carried out in triplicates with results expressed as mean±standard error. Statistically significant differences were calculated using the two-tailed unpaired one-way analysis of variance (ANOVA) with p values of ≤0.05, <0.01, and <0.001 considered significant using Prism 5.0 (GraphPad Software, CA, USA).

4.3 Results and Discussion

As shown in Figure 4-2, our TEM images clearly showed that all the NPs exhibited spherical shape with a well-defined diameter. Further, our DLS studies indicated that the hydrodynamic size of NPs was slightly higher than the dehydrated diameter obtained from a TEM. All the pristine NP suspensions exhibited high zeta potential suggesting long-term stability (Table 4.1).
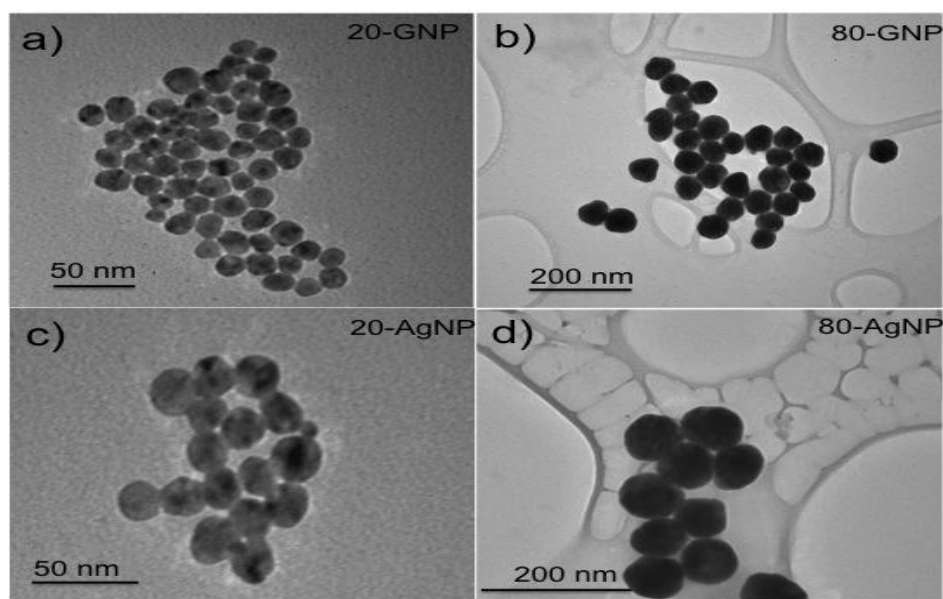

Figure 4-2. TEM micrographs of GNPs and AgNPs

Upon protein coating, the hydrodynamic size of all the NPs increased at least by ~10 nm. Furthermore, FBS coating resulted in a higher increase in hydrodynamic size compared to Alb possibly due to the adsorption of multiple proteins. The magnitude of the zeta potential of protein coated NPs decreased considerably indicating that the NPs agglomerate more rapidly due to the formation of protein coating, the hydrodynamic size of all the NPs increased at least by ~10 nm. Furthermore, FBS coating resulted in a higher increase in hydrodynamic size compared to Alb possibly due to the adsorption of multiple proteins. The magnitude of the zeta potential of protein coated NPs decreased considerably indicating that the NPs agglomerate more rapidly due to the formation of a protein corona.

The UV-Vis absorption spectra shown in Figure 4-3 displayed the characteristic surface plasmon resonance peak (SPR) at ~520-550 nm for GNPs and 400-420 nm for AgNPs. Interestingly, we observed that the SPR peak showed an evident upshift for all the protein coated NPs. Such an observation may be interpreted as follows. In metal NPs, the characteristic peak of SPR is dependent on the size, shape, and dielectric function(ϵ) of the NPs and its surrounding medium. In our case, the interaction of GNPs/AgNPs with protein molecules resulted in a further change of ϵ leading to an upshift in the extinction coefficient maximum and the SPR peaks.
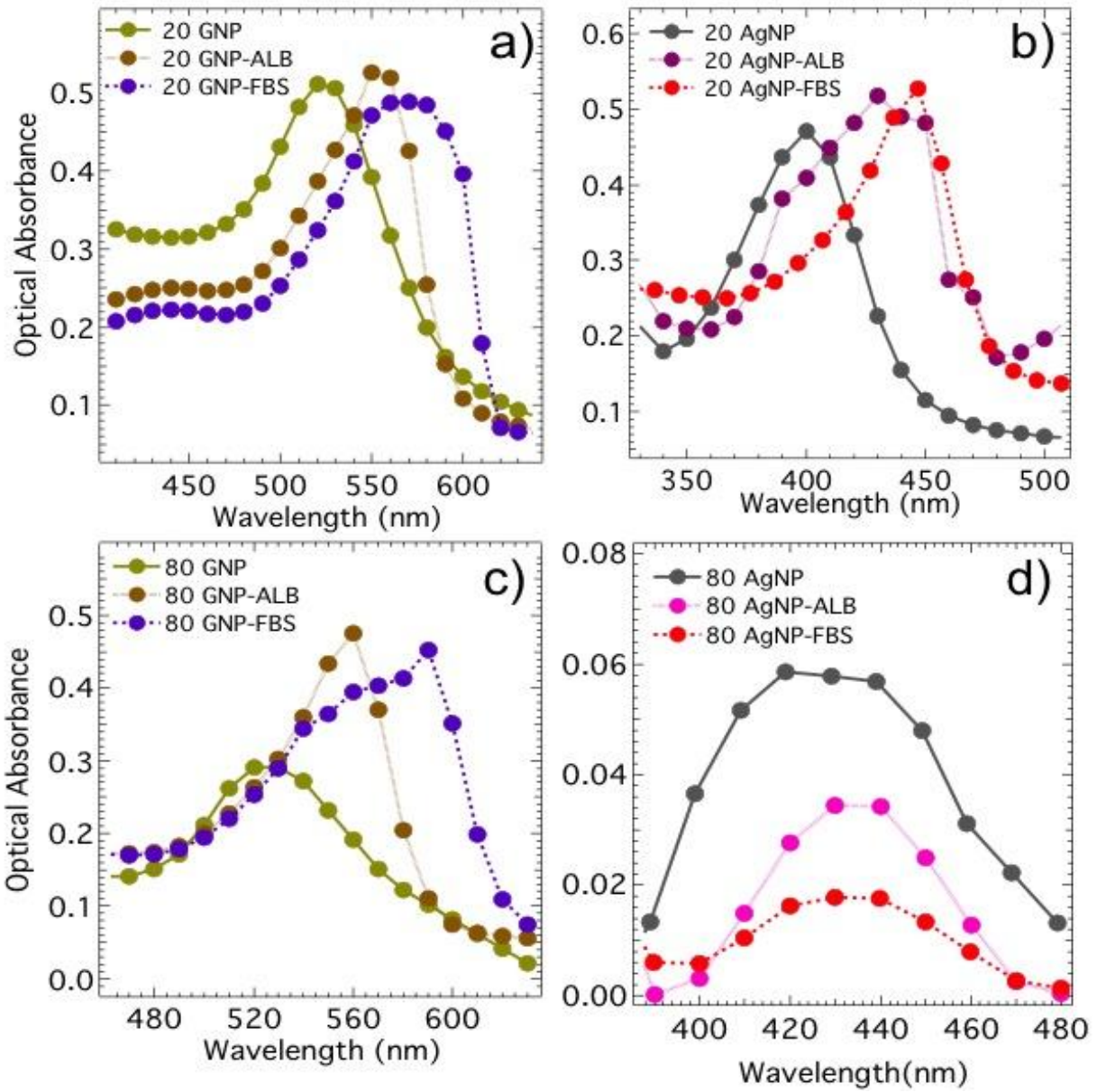
Figure 4-3 UV-Vis absorption spectrum of plain, ALB and FBS bound GNPs and AgNPs

Sample	Size(nm)	Zeta Poetential (mV)
20 GNP	20	-54.4
20 -GNP-ALB	30	-10.5
20 –GNP-FBS	41	-9.99
80 GNP	86	-28.8
80 – GNP- ALB	99	-8.65
80 –GNP-FBS	109	-9.51

Table 4-1. Hydrodynamic size and zeta potential of functionalized GNPs

Sample	Size (nm)	Zeta Potential (mV)
20 -AgNP	20	-43.2
20 –AgNP-ALB	33	-13.9
20 –AgNP-FBS	43	-10.2
80 -AgNP	80	-48.45
80 –AgNP-ALB	110	-14
80 –AgNP-FBS	123	-9.59

Table 4-2 Hydrodynamic size and zeta potential of functionalized AgNPs

The above experiments were done in our lab. The experiments and results mentioned below were conducted in Dr. Jeremy Zhang's lab.

The percentage of apoptosis caused by 20-GNPs and 80-GNPs are depicted in Figure 4-5 (a). It was seen that 20-GNPs caused significantly more (P<0.001) apoptosis in MCF-7 and DU-145 cells than the HT-29 cells. The protein coated 20-GNPs in general showed a decrease in the percentage of apoptotic cells in MCF-7 cells when compared with plain 20-GNPs Figure 4-5 (a). On the other hand, 80-GNPs caused significant cytotoxicity in DU-145 cells than MCF-7 and HT-29 cells Figure 4-5(b). Significant apoptosis was characteristically higher in MCF-7 and DU-145 cells than the HT-29 cells. The ALB-80-GNPs caused 20% more apoptosis in MCF-7 and DU-145 cells than FBS-80-GNPs which caused significant apoptosis of about 25% in MCF-7 cells

and only 8% cytotoxicity in DU-145 cells. It is interesting to note that the HT-29 cells did show significantly low apoptotic cells when treated with ALB/FBS-80-GNPs as shown in Figure 4-5 (b).

As shown in Figure 4-5 (c) the 20-AgNPs and 80-AgNPs showed significant ($P<0.001$) cytotoxic effects in MCF-7 and DU-145 cells. The MCF-7 cells had significantly higher levels of apoptosis when treated with 20/80-AgNPs and as well as 20/80-ALB-AgNPs when compared to DU-145 and HT-29 cells Figure 4-5(c) &(d). In the case of HT-29 cells, there was a significant decrease in cytotoxicity when the cells were treated with plain AgNPs and FBS-AgNPs. Interestingly the 80-AgNPs brought about higher cytotoxicity than the 20-AgNPs. On the contrary, the FBS-80-AgNPs exhibited higher apoptosis in DU-145 cells when compared to ALB-80-AgNPs Figure 4-5 (d). The plain 80-GNPs showed significant apoptotic effects in HT-29 and DU-145 cells rather than the multi-drug resistant (MDR) MCF-7 cells.
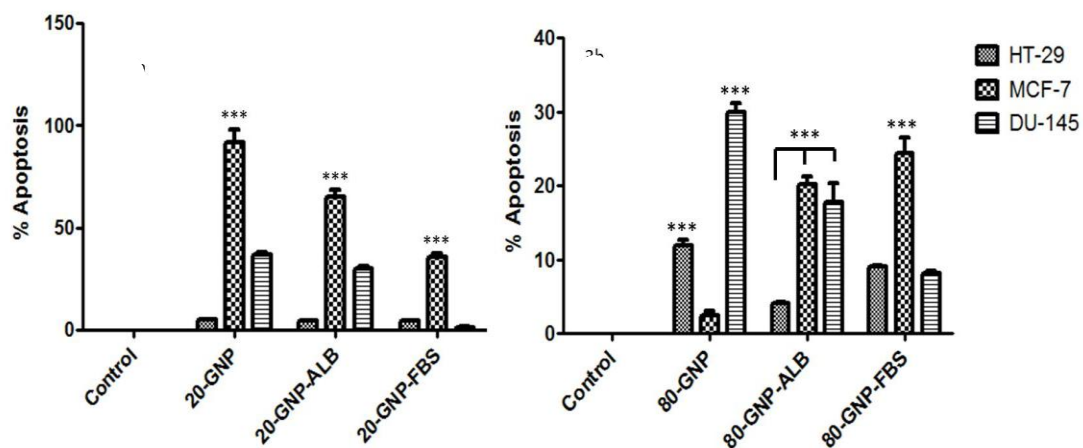
Figure 4-5 (a), (b). Percent apoptosis caused by GNPs
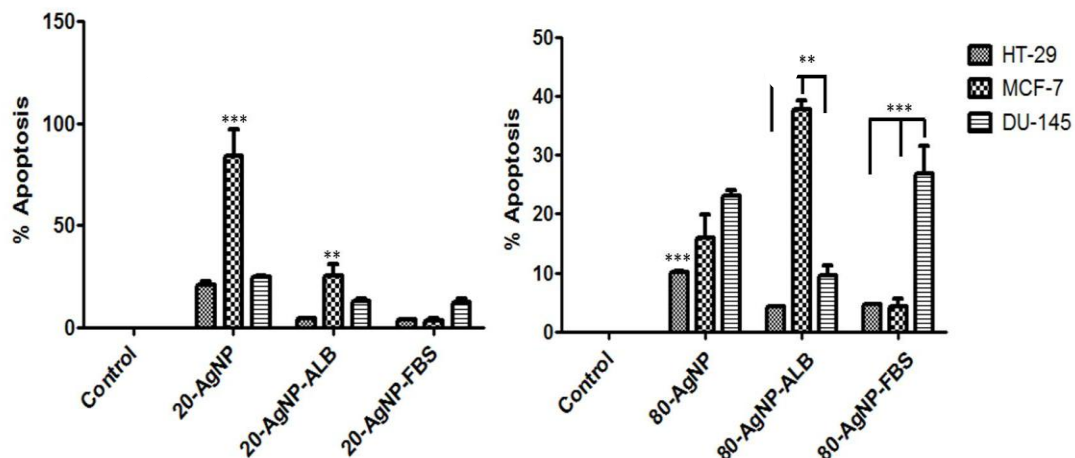
Figure 4.5 (c),(d). Percent apoptosis caused by AgNPs

APPENDIX

GLOSSARY OF TERMS USED IN THIS DISSERTATION

SWNT	Single walled carbon nanotube
MWNT	Multiwalled carbon nanotube
DNA	Deoxyribonucleic acid
RNA	Ribonucleic acid
TEM	Transmission Electron Microscopy
ENM	Environmentally based nanomaterials
NP-PC	Nanoparticle Protein Corona
CVD	Chemical Vapor Deposition
XPS	X-Ray Photoelectron Spectroscopy
FLG	Few-Layer Graphene
CCD	Charge Coupled Device
BSA	Bovine Serum Albumin
FBS	Foetal Bovine serum
ALB	Albumin
MDR	Multi-Drug Resistant

REFRENCES

1. Beddow, V. *Research Needs in Leachate Treatment for Remediation of Aquatic Environment*2010;Availablefrom:http://www.iwawaterwiki.org/xwiki/bin/view/Articles/tonni

2. *Nanotechnology information center: properties, applications, research, and safety quidlines*. Availablefrom:http://www.americanelements.com/nanotech.htm.

3. Maynard, A.D., *Nanotechnology: a research strategy for addressing risk* 2006; Availablefrom: http://www.pewtrusts.org/our_work_report_detail.aspx?id=19682.

4. Kroto, H.W., Allaf, A.W., and Balm, S.P., *C60: Buckminsterfullerene.* Chemical Reviews 1991. **91**(6): p. 1213-1235.

5. Heller, D.A., Jeng, E.S., Yeung, T.-K., Martinez, B.M., Moll, A.E., Gastala, J.B., and Strano, M.S., *Optical Detection of DNA Conformational Polymorphism on Single-Walled Carbon Nanotubes.* Science, 2006. **311**(5760): p. 508-511

6. Heller, D.A., Jeng, E.S., Yeung, T.-K., Martinez, B.M., Moll, A.E., Gastala, J.B., and Strano,M.S., *Optical Detection of DNA Conformational Polymorphism on Single-Walled Carbon Nanotubes.* Science, 2006. **311**(5760): p. 508-511

7. Pantarotto, D., Singh, R., McCarthy, D., Erhardt, M., Briand, J.-P., Prato, M., Kostarelos,K., and Bianco, A., *Functionalized Carbon Nanotubes for Plasmid DNA Gene Delivery.*Angewandte Chemie International Edition, 2004. **43**(39): p. 5242-5246

8. Pantarotto, D., Partidos, C.D., Graff, R., Hoebeke, J., Briand, J.-P., Prato, M., and Bianco.*Synthesis, Structural Characterization, and Immunological Properties of CarbonNanotubes Functionalized with Peptides.* Journal of the American Chemical Society,2003. **125**(20): p. 6160-6164

9. Pantarotto, D., Singh, R., McCarthy, D., Erhardt, M., Briand, J.-P., Prato, M., Kostarelos,K., and Bianco, A., *Functionalized Carbon Nanotubes for Plasmid DNA Gene Delivery.* Angewandte Chemie International Edition, 2004. **43**(39): p. 5242-5246

10. Pantarotto, D., Partidos, C.D., Graff, R., Hoebeke, J., Briand, J.-P., Prato, M., and Bianco.,*Synthesis, Structural Characterization, and Immunological Properties of Carbon Nanotubes Functionalized with Peptides.* Journal of the American Chemical Society,2003. **125**(20): p. 6160-6164

11. Wu, W., Wieckowski, S., Pastorin, G., Benincasa, M., Klumpp, C., Briand, J.P., Gennaro,R., Prato, M., and Bianco, A., *Targeted delivery of amphotericin B to cells by using functionalized carbon nanotubes.* Angewandte Chemie (International ed. in English),2005. **44**(39): p. 6358-6362.

12. Ferrari, M., *Cancer nanotechnology: opportunities and challenges.* Nat Rev Cancer, 2005.**5**(3): p. 161-171

13. Chen, J., Chen, S., Zhao, X., Kuznetsova, L.V., Wong, S.S., and Ojima, I., *Functionalized Single-Walled Carbon Nanotubes as Rationally Designed Vehicles for Tumor-Targeted Drug Delivery.* Journal of the American Chemical Society, 2008. **130**(49): p. 16778-16785

14. *Tech report: Carbon nanotubes used to more easily detect cancer cells, HIV*. 2011;Available from: http://tech.resuck.com/2011/03/carbon-nanotubes-used-to-moreeasily-detect-cancer-cells-hiv/

15. Kroto, H.W., Heath, J.R., O'Brien, S.C., Curl, R.F., and Smalley, R.E., *C60: Buckminsterfullerene.* Nature, 1985. **318**(6042): p. 162-163

16. Kroto, H.W., Allaf, A.W., and Balm, S.P., *C60: Buckminsterfullerene.* Chemical Reviews,1991. **91**(6): p. 1213-1235

17. Yoon, S.H., Lim, S., Hong, S.-h., Mochida, I., An, B., and Yokogawa, K., *Carbon nano-rod as a structural unit of carbon nanofibers.* Carbon, 2004. **42**(15): p. 3087-3095.

18. Service, R.F., *Carbon Foam Reveals a Fleeting Magnetic Personality.* Science, 2004.**304**(5667): p. 42-42.

19. Sun, Y.P., Zhou, B., Lin, Y., Wang, W., Fernando, K.A.S., Pathak, P., Meziani, M.J., Harruff, B.A., Wang, X., Wang, H., Luo, P.G., Yang, H., Kose, M.E., Chen, B., Veca, L.M., and Xie, S.-Y., *Quantum-Sized Carbon Dots for Bright and*

Colorful Photoluminescence. Journal of the American Chemical Society, 2006. **128**(24): p. 7756-7757.

20. Bandow, S., Kokai, F., Takahashi, K., Yudasaka, M., Qin, L.C., and Iijima, S., *Interlayerspacing anomaly of single-wall carbon nanohorn aggregate.* Chemical Physics Letters,2000. **321**(5-6): p. 514-519.

21. King, M.A., *Detection of dead cells and measurement of cell killing by flow cytometry.*Journal of Immunological Methods, 2000. **243**(1-2): p. 155-166.

22. Schrand, A.M., Huang, H., Carlson, C., Schlager, J.J., Ōsawa, E., Hussain, S.M., and Dai, L.,*Are Diamond Nanoparticles Cytotoxic?* The Journal of Physical Chemistry B, 2006.**111**(1): p. 2-7.

23. Lewinski, N., Colvin, V., and Drezek, R., *Cytotoxicity of Nanoparticles.* Small, 2008. **4**(1) p. 26-49.

24. Novoselov, K. S., Geim, A K., Morozov, S. V.,Jiang, D, Zhang, Y.,Dubonos, S V.,Griegoriva, I.Firsov,*Science* **2004,** *306, 666-669*

25. Novoselov, K. S.; Jiang, D.; Schedin, F.; Booth, T. J.; Khotkevich, V. V.; Morozov, S. V.; Geim, A K. *Proc. Natl. Acad. Sci.* **2005**, *102*, 10451-3.

26. . Zhang, Y.; Small, J. P.; Pontius, W. V.; Kim, P. *Appl. Phys. Lett.* **2005**, *86*, 073104.

27. . Blake, P.; Hill, E. W.; Castro Neto, A. H.; Novoselov, K. S.; Jiang, D.; Yang, R.; Booth, T. J.; Geim, A. K. *Appl. Phys. Lett.* **2007**, *91*, 063124.

28. Soldano, C.; Mahmood, A.; Dujardin, E. *Carbon* **2010**, *48*, 2127-2150.

29. Neugebauer, P.; Orlita, M.; Faugeras, C.; Barra, A.-L.; Potemski, M. *Phys. Rev. Lett.* **2009**, *103*, 2-5.

30. Perdigao L.M.A. Sabki, S. N.; Garfitt, J. M.; Capiod, P.; Beton, P. H. *J. Phys.Chem. C* **2011**, *115*, 7472-7476.

31. Forbeaux, I.; Themlin, J.; Debever, J. *Surf. Sci.* **1999**, *442*, 9-18.

32. Sutter, P. *Nat. Mater.* **2009**, *8*, 171-172.

33. Hass, J.; Feng, R.; Li, T.; Li, X.; Zong, Z.; de Heer, W. A.; First, P. N.; Conrad, E.H.; Jeffrey, C. A.; Berger, C. *Appl.Phys. Lett.* **2006**, *89*, 143106.

34. Emtsev, K. V.; Bostwick, A.; Horn, K.; Jobst, J.; Kellogg, G. L.; Ley, L.;McChesney, J. L.; Ohta, T.; Reshanov, S. A; Röhrl, J.; Rotenberg, E.; Schmid, A.K.; Waldmann, D.; Weber, H. B.; Seyller, T. *Nat. Mater.* **2009**, *8*, 203-7.

35. Park, S.; Ruoff, R. S. *Nat. Nanotech.* **2009**, *4*, 217-24.

36. Lerf, A.; He, H.; Forster, M. *J. Phys. Chem. B* **1998**, *5647*, 4477-4482.

37. He, H.; Riedl, T.; Lerf, A. *J. Phys. Chem. B* **1996**, *3654*, 19954-19958.

38. Buchsteiner, A.; Lerf, A.; Pieper, *J. Phys. Chem. B* **2006**, *110*, 22328-38.

39. Bose, S.; Kuila, T.; Mishra, A. K.; Kim, N. H.; Lee, J. H. *Nanotechnology* **2011**, *22*,405603.

40. An, X.; Simmons, T.; Shah, R.; Wolfe, C.; Lewis, K. M.; Washington, M.; Nayak, S.K.; Talapatra, S.; Kar, S. *Nano letters* **2010**, *10*, 4295-301.

41. Jiao, L.; Zhang, L.; Wang, X.; Diankov, G.; Dai, H. *Nature* **2009**, *458*, 877-80.

42. Luo, Z.; Lu, Y.; Singer, D. W.; Berck, M. E.; Somers, L. A.; Goldsmith, B. R.;Johnson, A. T. C. *Chem. Mater.* **2011**, *23*,1441-1447.

43. Liu, W.; Li, H.; Xu, C.; Khatami, Y.; Banerjee, K. *Carbon* **2011**, *49*, 4122-4130.

44. Alexis, F., J.-W. Rhee, et al. (2008). *New frontiers in nanotechnology for cancer treatment*. Urologic Oncology: Seminars and Original Investigations 26(1): 74-85.

45. Asha Rani, P. V., G. Low Kah Mun, et al. (2009). *Cytotoxicity and genotoxicity of silver nanoparticles in human cells.* ACS Nano 3(2): 279-290.

46. Capriotti, A. L., G. Caracciolo, et al. (2011). *Differential analysis of "protein corona" profile adsorbed onto different nonviral gene delivery systems*. Anal Biochem 419(2): 180-189.

47. Capriotti, A. L., G. Caracciolo, et al. (2011). *DNA affects the composition of lipoplex protein corona: a proteomics approach.* Proteomics 11(16): 3349-3358.

48. Caracciolo, G., D. Pozzi, et al. (2011). *Evolution of the protein corona of lipid gene vectors as a function of plasma concentration*. Langmuir 27(24): 15048-15053.

49. Dizdaroglu, M. (1992). *Oxidative damage to DNA in mammalian chromatin*. Mutat Res 275(3-6): 331-342.

50. Heller, M. and M. J. Heller (2006). *Nanotechnology for cancer diagnostics and therapeutics* Nanomedicine: Nanotechnology, Biology and Medicine 2(4): 301.

51. Hu, J. J., N. Dubin, et al. (1995). *The effects of hydrogen peroxide on DNA repair activities.* Mutation Research/DNA Repair 336(2): 193-201.

52. Kasten, B. B., T. C. Liu, et al. (2013).*Targeting prostate cancer cells with PSMA inhibitor-guided gold nanoparticles.* Bioorganic & Medicinal Chemistry Letters 23(2): 565-568.

53. Katsnelson, B. A., L. I. Privalova, et al. (2013). *Comparative in vivo assessment of some adverse bioeffects of equidimensional gold and silver nanoparticles and the attenuation of nanosilver's effects with a complex of innocuous bioprotectors*. Int J Mol Sci 14(2): 2449-2483.

54. Kumar, S., N. Harrison, et al. (2007). *Plasmonic Nanosensors for Imaging Intracellular Biomarkers in Live Cells* Nano Letters 7(5): 1338-1343.

55. Lundqvist, M., J. Stigler, et al. (2011). *The Evolution of the Protein Corona around Nanoparticles: A Test Study.* ACS Nano 5(9): 7503-7509.

56. Mirshafiee, V., M. Mahmoudi, et al. (2013). *Protein corona significantly reduces active targeting yield.* Chem Commun (Camb) 49(25): 2557-2559.

57. Mohan, J. C., G. Praveen, et al. (2013). *Functionalised gold nanoparticles for selective induction of in vitro apoptosis among human cancer cell lines.* Journal of Experimental Nanoscience 8(1): 32-45.

58. Park, M. V., A. M. Neigh, et al. (2011). *The effect of particle size on the cytotoxicity, inflammation, developmental toxicity and genotoxicity of silver nanoparticles*. Biomaterials 32(36): 9810-9817.

59. Podila, R. and J. M. Brown (2013). *Toxicity of engineered nanomaterials: a physicochemical perspective*. J Biochem Mol Toxicol 27(1): 50-55.

60. Podila, R., P. Vedantam, et al. (2012). *Evidence for Charge-Transfer-Induced Conformational Changes in Carbon Nanostructure–Protein Corona*. The Journal of Physical Chemistry C 116(41): 22098-22103.

61. Reed, J. C. Mechanisms of apoptosis, Am J Pathol. 2000 Nov;157(5):1415-30. Schaffler, M., M. Semmler-Behnke, et al. (2013). *Serum protein identification and quantification of the corona of 5, 15 and 80 nm gold nanoparticles*. Nanotechnology 24(26): 265103.

62. Selim, M. E. and A. A. Hendi (2012). *Gold Nanoparticles Induce Apoptosis in MCF-7 Human Breast Cancer Cells*. Asian Pacific Journal of Cancer Prevention 13(4): 1617-1620.

63. Singh, R. P. and P. Ramarao (2012). *Cellular uptake, intracellular trafficking and cytotoxicity of silver nanoparticles*. Toxicol Lett 213(2): 249-259.

64. Sobhan, M. A., V. K. A. Sreenivasan, et al. (2012). *Non-specific internalization of laser ablated pure gold nanoparticles in pancreatic tumor cell*. Colloids and Surfaces B: Biointerfaces 92(0): 190-195.

65. Sudimack, J. and R. J. Lee (2000). *Targeted drug delivery via the folate receptor."* Advanced Drug Delivery Reviews 41(2): 147-162.

66. Thakkar, K. N., S. S. Mhatre, et al. (2010). *Biological synthesis of metallic nanoparticles*. Nanomedicine: Nanotechnology, Biology and Medicine 6(2): 257-262.

67. Vedantam, P., G. Huang, et al. (2013). *Size-dependent cellular toxicity and uptake of commercial colloidal gold nanoparticles in DU-145 cells*. Cancer Nanotechnology: 1-8.